


# Differentiation of large extracellular vesicles in oral fluid: Combined protocol of small force centrifugation and sedimentation pattern analysis

Takamasa Kawano<sup>1,2</sup> | Kohji Okamura<sup>3</sup> | Hiroki Shinchi<sup>4</sup> | Koji Ueda<sup>4</sup> | Takeshi Nomura<sup>2</sup> | Kiyotaka Shiba<sup>1</sup> 

<sup>1</sup>Division of Protein Engineering, Cancer Institute, Japanese Foundation for Cancer Research, Koto-ku, Tokyo, Japan

<sup>2</sup>Department of Oral Oncology, Oral and Maxillofacial Surgery, Tokyo Dental College, Ichikawa, Chiba, Japan

<sup>3</sup>Department of Systems BioMedicine, National Center for Child Health and Development, Setagaya-ku, Tokyo, Japan

<sup>4</sup>Cancer Precision Medicine Center, Japanese Foundation for Cancer Research, Koto-ku, Tokyo, Japan

## Correspondence

Kiyotaka Shiba, Division of Protein Engineering, Cancer Institute, Japanese Foundation for Cancer Research, 3-8-31, Ariake, Koto-ku, Tokyo 135-8550, Japan.

Email: [kshiba@jfc.or.jp](mailto:kshiba@jfc.or.jp)

## Funding information

JSPS Grant-in-Aid for Scientific Research (B), Grant/Award Number: 20H03538

## Abstract

Extracellular vesicles (EVs) in biofluids are highly heterogeneous entities in terms of their origins and physicochemical properties. Considering the application of EVs in diagnostic and therapeutic fields, it is of extreme importance to establish differentiating methods by which focused EV subclasses are operationally defined. Several differentiation protocols have been proposed; however, they have mainly focused on smaller types of EVs, and the heterogeneous nature of large EVs has not yet been fully explored. In this report, to classify large EVs into subgroups based on their physicochemical properties, we have developed a protocol, named EV differentiation by sedimentation patterns (ESP), in which entities in the crude large EV fraction are first moved through a density gradient of iodixanol with small centrifugation forces, and then the migration patterns of molecules through the gradients are analysed using a non-hierarchical data clustering algorithm. Based on this method, proteins in the large EV fractions of oral fluids clustered into three groups: proteins shared with small EV cargos and enriched in immuno-related proteins (Group 1), proteins involved in energy metabolism and protein synthesis (Group 2), and proteins required for vesicle trafficking (Group 3). These observations indicate that the physicochemical properties of EVs, which are defined through low-speed gradient centrifugation, are well associated with their functions within cells. This protocol enables the detailed subclassification of EV populations that are difficult to differentiate using conventional separation methods.

## KEYWORDS

EVs, large EVs, saliva, subclassification

## 1 | INTRODUCTION

Extracellular vesicles (EVs) are defined in Minimal Information for Studies of Extracellular Vesicles (MISEV) 2018 (Théry et al., 2018) as the collective term for particles released from cells that are delineated by lipid bilayer(s) and cannot replicate by themselves. Cells have many routes to generate EVs, including multivesicular body-mediated pathways (Johnstone, 2005; Raposo et al., 1996), protrusion-originated productions (Rilla, 2021; Sung et al., 2021), and regulated cell death-related secretion (Poon et al., 2019). Thus, EVs contained in biofluids are quite heterogeneous populations originating from different cell types as well as distinct generation pathways (Buzas, 2023; Colombo et al., 2014; van Niel et al., 2018).

This is an open access article under the terms of the [Creative Commons Attribution-NonCommercial License](https://creativecommons.org/licenses/by-nc/4.0/), which permits use, distribution and reproduction in any medium, provided the original work is properly cited and is not used for commercial purposes.

© 2024 The Authors. *Journal of Extracellular Biology* published by Wiley Periodicals, LLC on behalf of the International Society for Extracellular Vesicles.

EVs have been proposed to be involved in normal cells/organs differentiation as well as in the development and progression of various diseases (Lischning et al., 2022; Salomon et al., 2022). Although small types of EVs have been gathering attention as responsible agents for these biological activities, quite a few researchers have also focused on larger EVs as central executants of biological activities (Anderson, 1969; Kilinc et al., 2021; Kowal et al., 2016; Melentijevic et al., 2017; Raposo et al., 1996; Weems et al., 2023). Here, the sizes of EVs (small or large) can be quantitatively determined from certain measurement methods, such as nanoparticle tracking analysis, resistive pulse sensing, atomic force micrography, and transmission electron microscopy, after being differentiated by sequential centrifugation, gel filtration, field-flow fractionation, or other methods (Théry et al., 2018). However, the sizes of EVs themselves do not necessarily provide information about their origins in terms of parental cells and generation routes. For example, it is often noted that small, medium, and large sizes of EVs are generated, respectively, through multivesicular body-mediated secretion, budding from the plasma membrane, and apoptotic cell burst. However, membrane budding and apoptosis have been shown to produce small EVs (Crescitelli et al., 2020; Poon et al., 2019) as well as large ones, exemplifying the limitation of size-based subclassification of EVs.

In our previous work (Hiraga et al., 2021), we captured a whole picture of EVs contained in healthy and oral cancer patients' oral fluids (OFs) using pentapartite differential centrifugation, in which OFs were fractionated into five sub-populations through sequential centrifugation at 300 (0.3K), 2000 (2K), 10,000 (10K), and 160,000 (160K) g, with the 2 and 160K fractions enriched with large (100 nm ~ several  $\mu$ m observed in transmission electron microscopy) and small EVs ( $52.7 \pm 30.7$  nm by nanoparticle tracking analysis), respectively. From the characterizations of each fraction, we found prominent alterations in the 2K fraction of patients' OFs in terms of the amounts and the sizes of certain protein markers, which suggested that diagnostic information can be drawn not only from small but also from large EVs (Hiraga et al., 2021). To explore this possibility, we must first further differentiate the 2K fraction using certain defined operational manipulations, because the fractions obtained by sequential centrifugations are still very heterogeneous and can be further subclassified using other methods. For small EVs, an equilibrium density gradient centrifugation is often used for this purpose, in which EVs float from the bottom or sediment from the top through a density gradient medium until their densities agree with those of the surrounding medium (Supplementary Information 1). Although only a portion of EVs migrate to their equilibrium positions under standard conditions (Aalberts et al., 2012; Iwai et al., 2016; Palma et al., 2012; Yamamoto et al., 2021), this methodology has been frequently used to sort heterogeneous small EVs into subclasses with distinct densities. The key point to note for equilibrium density gradient centrifugation is that the information for the sizes of EVs is discarded at equilibrium conditions (Supplementary Information 1). In our previous observation, the large EVs contained in the 2K fraction varied in size compared to the small EVs in the 160K fraction, which suggested that we employ non-equilibrium conditions for differentiating large EVs. In this study, we propose a new protocol for differentiating large EVs, in which crude large EVs are first sedimented through density gradients at low speeds and short times, and then the migration patterns of molecules are analysed using a non-hierarchical data clustering algorithm. We named this differentiation protocol *EV differentiation by sedimentation patterns* (ESP). In this study, large EVs are primarily defined as the subtypes of EVs found in the 2K fraction, following our previous study (Hiraga et al., 2021). Nevertheless, our findings in this investigation revealed that the 2K fraction also contains smaller EVs, which might associate with larger EVs and, consequently, exhibit the behaviours of larger particles during the centrifugation process. This association underscores the inherent challenges in establishing operational definitions for EV subtypes as it complicates the clear delineation between 'large' and 'small' classifications.

## 2 | MATERIALS AND METHODS

### 2.1 | Oral fluid collection

The OF samples were collected from three healthy volunteers with informed consent, as described previously (Hiraga et al., 2021). Briefly, 40 mL of oral fluid was expectorated into plastic tubes ( $2 \times 20$  mL) (430829, Corning, NY, USA) placed on ice. Volunteers were prohibited from eating, drinking, and brushing for 1 h prior to collection, which began at 9:00 AM. The subjects were all males aged 28, 30, and 64 years old who did not receive any dental treatment within 48 h. The collected OFs were flash frozen in liquid nitrogen, stored at  $-80^{\circ}\text{C}$ , and thawed at  $4^{\circ}\text{C}$  for use in EV isolation. Ethical approval was obtained from the Tokyo Dental College of Ethics Committee (approval number:1-16-46RIV) and the Japanese Foundation for Cancer Research (approval number: JFCR 2016-1125).

### 2.2 | Differentiation of the 2K fraction

To prepare the 2K fraction, 20 mL of frozen OFs were thawed, and debris was removed by centrifugation at 300 g for 10 min (model 5500, Kubota, Osaka, Japan). The resultant supernatant was then centrifuged at 2000 g for 10 min, and the pellets were dissolved in 5 mL of phosphate-buffered saline (PBS, 137 mM NaCl, 2.68 mM KCl, 8.10 mM  $\text{Na}_2\text{HPO}_4$ , 1.47 mM  $\text{KH}_2\text{PO}_4$ , pH

7.4) and centrifuged under the same conditions to obtain the pellet of the 2K fraction. All centrifugations were done at 4°C. In this study, we omitted the sonication step prior to 300 g centrifugation, which was employed in the pentapartite analyses (Hiraga et al., 2021), because it was only needed for the density gradient centrifugation of small EVs (Iwai et al., 2016) and did not affect the properties of the 2K fraction (unpublished result). A continuous density gradient of 8%–48% iodixanol (OptiPrep, 1114542, Shield PoC, Oslo, Norway) in 0.02 M HEPES ([4-(2-hydroxyethyl)-1-piperazine ethanesulfonic acid]/NaOH, pH 7.2) was prepared with a gradient mixer No. 3 (SAN4024, Sanplatec, Osaka, Japan) in a 10 mL tube (361707, Beckman Coulter). The 2K fraction was placed on the top or bottom of the media after dissolving the pellet in 500  $\mu$ L of 8% or 48% iodixanol in 0.02 M HEPES, respectively. Centrifugations were performed under the various conditions indicated in the RESULTS section using JXN-30 with a JS-24.38 rotor (Beckman Coulter). After centrifugation, nine individual 1 mL fractions were collected from the top, and the density of each fraction was measured using a refractometer (RX-5000a, Atago Co. Ltd, Tokyo, Japan). Only fraction 10 (bottom) was 0.5 mL of the sample. All samples were flash frozen in liquid nitrogen, stored at  $-80^{\circ}\text{C}$ , and thawed at 4°C before analysis.

### 2.3 | Pentapartite fractionation

Pentapartite fractionations of OFs were performed as described by Hiraga et al. (Hiraga et al., 2021), with slight modifications. Briefly, 5 mL of thawed OFs were sonicated with a closed-type sonication system (UCD-200T, Biorupter, Diagenode Inc., NJ, USA) and were sequentially centrifuged at 300 g for 10 min (model 5500 with tube 430829, CORNING), at 2000 g for 10 min (model 5500), at 10,000 g for 30 min (JXN-30 with JS-24.38 rotor and tube 364772, Beckman Coulter), and at 100,000 g for 110 min (JXN-30 with JS-24.38, 364772) to obtain the 0.3K, 2K, 10 and 100K fractions, respectively. The differences between the previous study (Hiraga et al., 2021) and the method described here are as follows: (i) the final pellet was obtained from 100,000 g for 110 min with a JS-24.38 rotor (k factor = 334) in this study instead of 160,000 g for 70 min with an SW32Ti rotor (k factor = 204) because of the availability of equipment; (ii) the pellets obtained from the first 300 g, 2000 g, 10,000 g and 100,000 g centrifugation were washed once by dissolving the pellets in 5 mL (for the 0.3 and 2K fractions) or 30 mL (for the 10 and 100K fractions) of PBS, followed by centrifugation under identical conditions to reduce carry-over of preceding fractions; and (iii) 10 mL of the final supernatant (Sup) was dialyzed against 1,000 mL of Milli-Q IQ 7010 purification system (Merck, Darmstadt, Germany) water using a Slide-A-Lyzer Dialysis Cassette (66110, Thermo Fisher Scientific, MA, USA) at 4°C for 24 h by exchanging external water four times, followed by lyophilization with FREEZONE 4.5 (FZ-4.5CL, Asahi Life Science, Saitama, Japan) for 18 h to prepare the concentrated Sup fraction in 152  $\mu$ L of PBS. All centrifugations were done at 4°C.

### 2.4 | Transmission electron microscopy

Transmission electron microscopy (TEM) observations were outsourced to Tokai Electron Microscopy, Inc. (Nagoya, Japan), where the samples were absorbed to formvar film-coated copper grids and stained with 2% phosphate tungstic acid solution (pH 7.0) for 30 s. The grids were observed by a transmission electron microscope (JEM-1400Plus; JEOL Ltd., Tokyo, Japan) at an acceleration voltage of 100 kV. Digital images (3296  $\times$  2472 pixels) were taken with a CCD camera (EM-14830RUBY2; JEOL Ltd.). Particle size was calculated using the Analyze Particles tool in ImageJ (<https://imagej.nih.gov/ij/>).

### 2.5 | Nanoparticle tracking analysis

The numbers and sizes of the particles were measured by nanoparticle tracking analysis (NTA) using a NanoSight LM10 system (Malvern Instruments, Worcestershire, UK), as previously reported (Hiraga et al., 2021). For pentapartite analyses, the 10 K fraction was calibrated with 150 nm diameter silica beads (24320, Polysciences, PA, USA), and 100 nm diameter beads (24041, Polysciences) were used for the 100 K fraction and supernatant. The camera level (CL) and detection threshold (DT) were set to CL 12/DT 10 and CL 14/DT 4. The samples were suspended in PBS filtered through a 0.1  $\mu$ m syringe filter (6789-1301, GE Healthcare UK Ltd., Buckinghamshire, UK) and diluted to achieve the desired concentration between  $2 \times 10^8$  and  $1 \times 10^9$  particles/mL. For each sample, 30 s of capture were recorded per sample, and each measurement was performed five times independently. NTA software version 2.3 (Malvern Instruments) was used for the data analysis, and average histograms were plotted from the five measurements. Differentiated 2K fractions were measured according to the 100K fraction.

## 2.6 | Mass spectrometry (MS)

We separated 600  $\mu\text{L}$  each of the 10 fractions using a gradient of iodixanol (see 2.2), mixed the aliquots with 400  $\mu\text{L}$  of PBS, and centrifuged them at 125,000  $g$  (45,000 rpm) for 70 min (Optima Max TL with TLA-55 rotor, Beckman Coulter). The resultant sediment was dissolved in 40  $\mu\text{L}$  of PBS and its protein concentration was estimated by a bicinchoninic acid (BCA) assay kit (23228, 1859078, Thermo Fisher Scientific, Waltham, MA, USA), using bovine serum albumin (23209, Thermo Fisher Scientific) as a standard. Mass spectrometric analysis of the protein samples was performed as described previously (Yamamoto et al., 2021). Briefly, the samples were concentrated using the 2-D Clean-Up Kit (80648451, GE Healthcare, Chicago, IL), reduced in  $1 \times$  Laemmli's sample buffer (32.9 mM Tris HCl, pH 6.8, 13.15% glycerol, 1.05% sodium dodecyl sulfate (SDS), 0.005% bromophenol blue) containing 10 mM Tris (2-carboxyethyl) phosphine for 10 min at 100°C, alkylated with 50 mM iodoacetamide at room temperature for 45 min, and subjected to SDS polyacrylamide gel electrophoresis (SDS-PAGE). The electrophoresis was stopped 2 mm from the top edge of the separation gel. After Coomassie Brilliant Blue staining, the protein bands were cut out, destained, cut into small pieces, and subjected to in-gel digestion with trypsin/Lys-C Mix (V5071, Promega, Madison, WI, USA) at 37°C for 12 h. The resulting peptides were extracted from the gel pieces and analysed using an Orbitrap Fusion Lumos mass spectrometer (Thermo Fisher Scientific, Waltham, MA) in combination with an UltiMate 3000 RSLC nanoflow HPLC (Thermo Fisher Scientific). MS/MS spectra were searched using the SwissProt *Homo sapiens* protein sequence database with Proteome Discoverer 2.5 software (Thermo Fisher Scientific).

## 2.7 | SDS-PAGE, western blot, and gel staining

For SDS-PAGE, 8  $\mu\text{L}$  of sample from each fraction was incubated with 6  $\mu\text{L}$  of reducing sample buffer (250 mM Tris HCl, pH 6.8, 20% sucrose, 8% SDS, 5% 2-mercaptoethanol, 0.008% bromophenol blue) and 10  $\mu\text{L}$  0.05% 2-methacryloyloxyethyl phosphorylcholine (MPC) polymer (Lipidure-BL802, NOF Corporation, Tokyo, Japan) and boiled at 90°C for 10 min (MPC polymer was added as signal enhancer). Proteins were separated on a 12.5% acrylamide gel (Extra PAGE One Precast Gel, 13074-34, Nacalai Tesque, Inc., Kyoto, Japan) using SDS running buffer (25 mM Tris, 191 mM glycine, 0.1% SDS) at a constant current of 500 V at 40 mA for 40 min. Separated proteins were then transferred onto 10 cm  $\times$  10 cm nitrocellulose membranes (IB201002, Invitrogen, CA, USA) using the iBlot dry blotting system (Invitrogen). After nonspecific binding sites were blocked by incubation in 10 mL of Blocking One (03953-95, Nacalai Tesque Corporation) for 1 h, the membrane was washed with 10 mL Tris-buffered saline-Tween [TBS-T, 10 mM Tris-HCl, 150 mM NaCl, 0.1% Tween-20 (P1379, Sigma-Aldrich)] three times for 5 min each, followed by incubation with antibody in 10 mL CanGet signal solution 1 (NKB-101, Toyobo, Osaka, Japan) for 120 min. The first antibody was probed by incubation with horseradish peroxidase-conjugated secondary antibodies in 10 mL of CanGet signal solution 2 for 60 min in the dark. All antibody incubations were performed using a gentle shaker. After each incubation step, the membranes were washed three times with 10 mL TBS-T for 5 min. Luminescence signals were obtained using an ECL system (A-8511, C-9008, Sigma-Aldrich) and visualized with a LumiVision LPR-130 (TAITEC, Saitama, Japan). For silver staining and Coomassie brilliant blue staining, Sil-Best Stain One (06865-81, Nacalai Tesque, Inc.) and InstantBlue (ISBIL, Expedeon, Cambridge, UK) were used, respectively. Antibodies used in western blotting experiments and their dilution rates were as follows: mouse anti-CD9 (SHI-EXO-M01, Cosmobio, Tokyo, Japan; 1:2000), mouse anti-CD63 (SHI-EXO-M02, Cosmobio; 1:1000), mouse anti-CD81 (SHI-EXO-M03, Cosmobio; 1:1000), rabbit anti-CD81 (66866-1-Ig, Proteintech, Rosemont, USA; 1:1000), goat anti-rabbit IgG (H + L)-HRP conjugate (170-6515, Bio-Rad, CA, USA; 1:2000), and goat anti-mouse IgG (H+L)-HRP conjugate (170-6516, Bio-Rad; 1:2000).

## 2.8 | Data analysis

The data obtained from the MS results were normalized with Microsoft Excel so that the maximum value was 1 and the minimum value was 0 for each protein. The average expression levels for each of the three samples was calculated. Cluster analysis was performed using TimeSeriesKMeans (a python package based on scikit-learn (Pedregosa, 2011), numpy (Harris et al., 2020), and scipy (Virtanen et al., 2020) published by tslearn (Tavenard et al., 2020), bioinfokit (Bedre, 2020), matplotlib (Hunter, 2007), seaborn (Waskom, 2021), and pandas (Reback et al., 2020). Subcellular localization and Gene Ontology analysis (Ashburner et al., 2000; Gene Ontology, 2021) were performed using metascape (Zhou et al., 2019).

## 2.9 | Reporting

We have submitted all relevant data to the EV-TRACK knowledgebase (EV-TRACK ID: EV220400) (Van Deun et al., 2017).

### 3 | RESULTS

#### 3.1 | Low-speed, short-time density gradient centrifugation raises the resolution of large EVs

Equilibrium density gradient centrifugation (isopycnic density gradient centrifugation) has often been used to differentiate small EVs from crude small EV fractions (Raposo et al., 1996). Theoretically, in this method, each EV particle moves through a density gradient medium from the top or from the bottom of the centrifugation tube to the position where the density of the particle becomes identical to that of the medium, and the velocity of the particle converges to zero (Supplementary Information 1). Previous studies, including ours, have, however, indicated that even after 96 h centrifugation, only a limited portion of small EVs reach their equilibrium state (Aalberts et al., 2012; Iwai et al., 2016; Palma et al., 2012; Yamamoto et al., 2021), indicating that particles present in the crude fraction did not behave as ideal spherical entities with distinct diameters. The observations also indicate that the non-equilibrium conditions of density gradient centrifugation (zonal density gradient centrifugation) can be used to differentiate heterogeneous EV populations based on their sizes as well as the densities of particles (Supplementary Information 1); that is, the size information of particles is not sacrificed in these conditions. This is suitable for characterizing the 2K fraction of OFs, because in our previous pentapartite analyses, TEM observations indicated that the particles contained in the 2K fraction had a wide range of sizes. For this reason, we first explored the non-equilibrium centrifugation conditions that separated EVs contained in the 2K fraction throughout the density gradient media.

According to Stokes' law, the effect of particle size should be more prominent with decreased rotational angular velocity (Supplementary Information 1). Therefore, we first sedimented the 2K fraction from the top of an 8%–48% iodixanol density gradient under three conditions: 2000 g for 1 h, 2000 g for 24 h, and 100,000 g for 1 h (Figure 1a). After centrifugation, 10 fractions were collected from the top, and each fraction was subjected to NTA analysis and silver staining (Figure 1b and Fig. S1). The NTA method determines the sizes of small particles based on their Brownian motion, and it simultaneously measures the number of particles (Carr et al., 2009), leading to its wide use in characterizing small EVs. However, the method has not been optimized for larger particles, and the presence of large particles in a sample hampers particle tracking (Dragovic et al., 2011; Théry et al., 2018; Van der Pol et al., 2014). In fact, in the analyses shown in Figure 1(a), fractions 3–10 of 2000 g for 1 h, and fractions 4–10 of 2000 g for 24 h and 100,000 g for 1 h contained larger particles that hindered the analyses in these fractions (shown by bars with asterisks in Figure 1b upper panels). By contrast, the top fractions of these samples were calculated to contain small particles by NTA, suggesting larger particles have moved toward the bottom of tubes in these centrifugation conditions. From the comparisons of NTA results obtained from the three conditions, we observed that particle dispersion increased with longer centrifugation time or higher centrifugal force, and the peak of particle concentration shifted from fraction 1 to 2 under these conditions. Silver-stained samples of fraction 5 had the strongest signals from all three conditions (Figure 1b), and a similar result was obtained when the sample floated up from the bottom (Figure 1c), suggesting that most but not all large EVs reached the equilibrium position (i.e., their density was 1.12–1.15 g/mL). To confirm that some EVs were in equilibrium with the medium after 2000 g of centrifugation for 1 h, the presence of aquaporin 5 (AQP5) in each fraction was investigated using western blotting. AQP5 has been thought to be exclusively expressed in salivary glands in the oral cavity (Ishikawa & Ishida, 2000). Reflecting this, in the pentapartite assay, AQP5 was barely detected in the 0.3K fraction, the major EV source of which may be derived from detached desquamated epithelium, blood cells, and bacteria. By contrast, the presence of AQP5 in both 2 and 160K fractions was evident, suggesting that AQP5 is secreted from salivary glands into the oral space as cargos of large and small EVs. When the 2K fraction was differentiated by density gradient centrifugation under four different conditions—2000 g for 1 h downward, 100,000 g for 1 h downward, 2000 g for 1 h upward, and 100,000 g for 1 h upward—the strongest signals were detected in fraction 5 for all conditions, indicating that most AQP5 was carried by large EVs, whose density was 1.12 g/mL, in the 2K fraction (Figure S2). In addition to the main signal, AQP5 was detected in the top or bottom fractions at 2000 g for 1 h downward or upward, respectively. The top or bottom signal migrated downward or upward, respectively, with a prolonged centrifugation time, suggesting that portions of AQP5 were also carried by smaller EVs in the 2K fraction (Figure S2). Assuming that the EVs that reached fraction 5 after 2000 g of centrifugation for 1 h reached density equilibrium, their diameter was calculated to be approximately 5  $\mu\text{m}$ . Another signal remained in fraction 1 at 2000 g for 1 h downward and moved to fraction 2 at 100,000 g for 1 h, suggesting that the diameter of the EV in fraction 2 was approximately 250 nm. If the particles with a diameter of 250 nm have a density of 1.12 g/mL (the canonical density of small EV (Raposo et al., 1996), Stokes' law (Supplementary Information 1) indicates that such particles would remain at the fraction under the conditions of 2000 g for 1 h. From these observations, we decided to use the conditions of 2000 g for 1 h downward to differentiate the 2K fraction, by which heterogeneous EVs in the 2K fractions can be separated through a density gradient based mainly on their sizes.

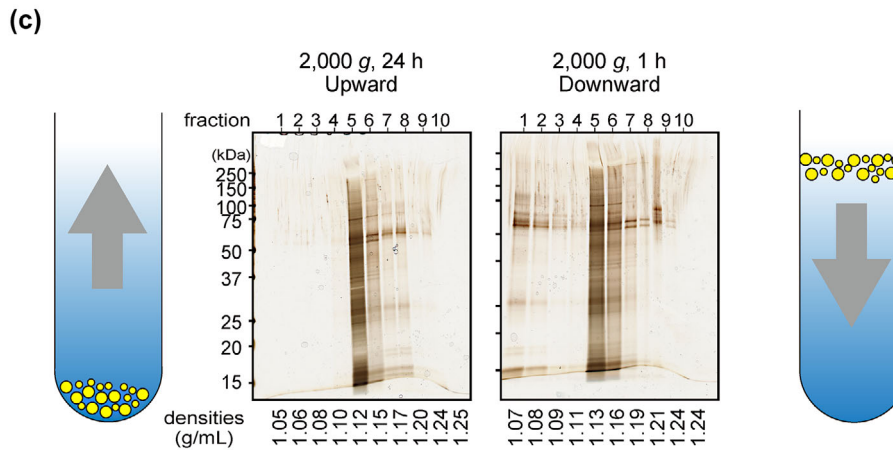
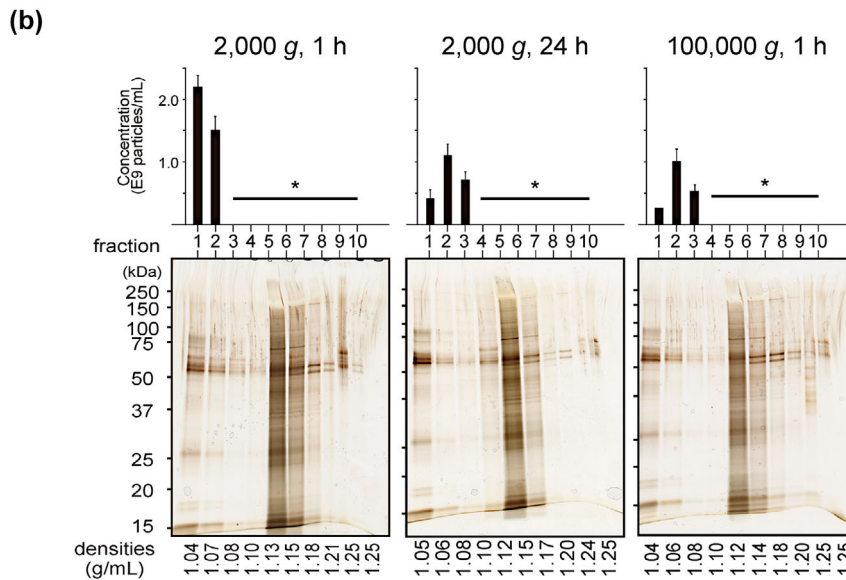
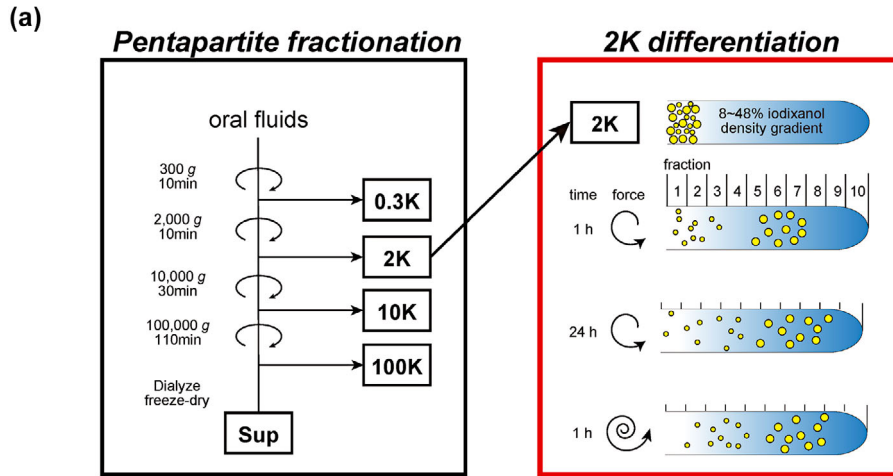


**FIGURE 1** Low-speed, short-time density gradient centrifugation raises the resolution of the 2K fraction. (a) Schematic representation pentapartite fractionation of OFs (left) and experiments to determine the centrifugation conditions for 2K (right). The details of pentapartite fractionation were described previously; however, in this study, the previous centrifugation condition of 160,000 g for 70 min (k factor = 204) was changed to 100,000 g for 30 min (k factor = 334) because of the availability of equipment. The 2K crude fraction was further differentiated through an 8%–48% iodixanol density gradient under three different conditions: 2000 g for 1 h, 2000 g for 24 h, and 100,000 g for 1 h. The length of the whorl in the right panel represents the strength of the centrifugal force. The yellow circles represent migrated particles having given sizes after centrifugations. (b) Concentrations of particles (upper) and silver staining of SDS-PAGE gels (bottom) of each of 10 fractions (upper) and silver staining after centrifugation under the three conditions. NTA analyses were performed five times, and the average and standard deviation are shown by black box and error bars. For fraction 1 of 100,000 g for 1 h, the NTA analyses were

(Continues)

**FIGURE 1** (Continued)

done only twice, thus the absence of an error bar. Fractions indicated by long horizontal bars with asterisks did not give concentrations because these fractions contained large particles whose sizes are outside the measurable range of NTA and hinder NTA analysis. Densities shown on the bottom of the gel were determined by refractometer. (c) Silver staining of SDS-PAGE gels for 10 fractions prepared under two different conditions. Under one condition (left), samples were floated from the bottom through gradient (upward) and under another condition (right), samples were sedimented from the top (downward).

### 3.2 | Do small EVs in the 2K fraction belong to the same class of small EVs in the 160K fraction?

As shown above, in the 2K fraction, AQP5 was carried by at least two distinct types of EV; one seems to be small and the other is large. This observation suggests the possibility that the large EVs containing AQP5 represent the secreted multivesicular bodies (MVBs), in which intraluminal vesicles (small EVs) carry AQP5. The small AQP5<sup>+</sup> EVs in 2K could have been those somehow released or leaked from the MVBs during the experimental procedures. Indeed, our study (Hiraga et al., 2021) and others' (Brody et al., 1983; Nonaka & Wong, 2017; Valcz et al., 2019) observations confirmed the presence of secreted MVB-like vesicles in bodily fluids.

To further explore this issue, we observed the particles contained in fractions 1, 5, and 7 using transmission electron microscopy (TEM) (Figure 2a), and their particle sizes were measured (Figure 2b, c). From fraction 1, small particles were mainly detected, whereas in fractions 5 and 7, much larger vesicles were detected. Unexpectedly, in fractions 5 and 7, not only large particles but also small particles were present (Figure 2a, c). The presence of small EVs in fractions 5 and 7 supports the possibility that these small EVs rapidly migrated to these fractions by associating with large EVs, or the small EVs might have assembled into large particles under the conditions of centrifugation (Linares et al., 2015).

CD9, CD63, and CD81 are other EV markers that have been detected in large EV fractions as well as small EVs (Hiraga et al., 2021; Kowal et al., 2016; Lischnig et al., 2022; Xu et al., 2016). In this work, we confirmed the wide distributions of these molecules with modified (see Materials and Methods) pentapartite analyses of OFs—that is, they were present on both a large EV fraction (2K) and a small EV fraction (100K) (Figure 2d). Further, we observed the following derivatives: (i) in the Sup fraction, CD9 gave the additional derivative (CD9-d1) whose apparent molecular weight was higher than the ones in other fractions, and (ii) anti-CD81 antibody detected high molecular weight (approximately 150 KDa; the origin of this high molecular weight signal was discussed in Figure S5) signal (CD81-HMW) in 0.3K, 2K, and Sup fractions, and the signals of the calculated molecular weight were most abundant in the Sup fractions). The 2K fractions of these three specimens were further differentiated by low-speed and short-time density gradient centrifugation, as described above (Figure 2e). Interestingly, CD9-d1, which was only detected in the Sup fraction in pentapartite analyses (Figure 2d), was detected after this centrifugation, and this CD9-d1 was only detected in fraction 1 (Figure 2e). The CD9 signal with calculated molecular weight was distributed with biphasic signals, whose peaks were fractions 1 and 5. CD63 exhibited monophasic distribution peaking in fraction 5. In the case of CD81, the signal with the calculated molecular weight was detected only from fraction 1, whereas CD81-HMW was detected from fractions 3 to 5. The fact that different forms of these molecules were detected from fractions 1 and 5 contradicts the simple scenario that a small EV in fraction 1 originated from the MVBs in fraction 5, as considered above. Combined with the data for AQP5 (Figure S2), these observations indicate that distinct classes of EVs are involved in carrying AQP5, CD9, and CD81 in OFs. In the case of CD9 and CD81, different forms of these molecules (CD9 and CD9-d1, as well as CD81 and CD81-HMW) are associated with distinct EVs, highlighting the complexity of EV differentiations.

### 3.3 | Classification of proteins in 2K based on their migration patterns

As shown above, the migration patterns of AQP5, CD9, and CD81 were biphasic, whereas that of CD63 was monophasic after low-speed and short-time density gradient centrifugation of the 2K fraction. We have observed various migration patterns in the proteins examined, and some are shown in Figure S3. VMPI1, which is involved in autophagosome formation (Ropolo et al., 2007), was mostly detected in fractions 3–5. This molecule has two forms, approximately 40 and 37K, and in one specimen, the 40K form was enriched in fraction 1, resembling the case of CD9. Further, ATP5A (a subunit of the mitochondrial ATP synthase) showed a monophasic distribution and was mainly detected in fraction 6 (Figure S3). We thought the different migration patterns through density gradient centrifugation at low speed and for a short time could offer information on their origins and decided to comprehensively examine the distributions of proteins among the 10 fractions using MS (a total of 3973 proteins from three OF specimens. Data are available upon request.). First, we analysed the obtained MS data using a standard hierarchical clustering method (Waskom, 2021), which did not resolve proteins into prominent sub-groups (Figure S4A). Next, we employed a hierarchical clustering method, TimeSeriesKMeans, which allows clustering on time-series data, such as electrocardiograms, and has been widely used for pattern analyses (Tavenard et al., 2020). For TimeSeriesKMeans analyses, the number of clusters had to be first determined, which we calculated to be three from our Silhouette analysis (Figure 3a) (Rousseeuw, 1987). Importantly, when we compared clustering numbers 2, 3, and 4, the three groups showed the most distinct patterns (Figure 3b, S4B).

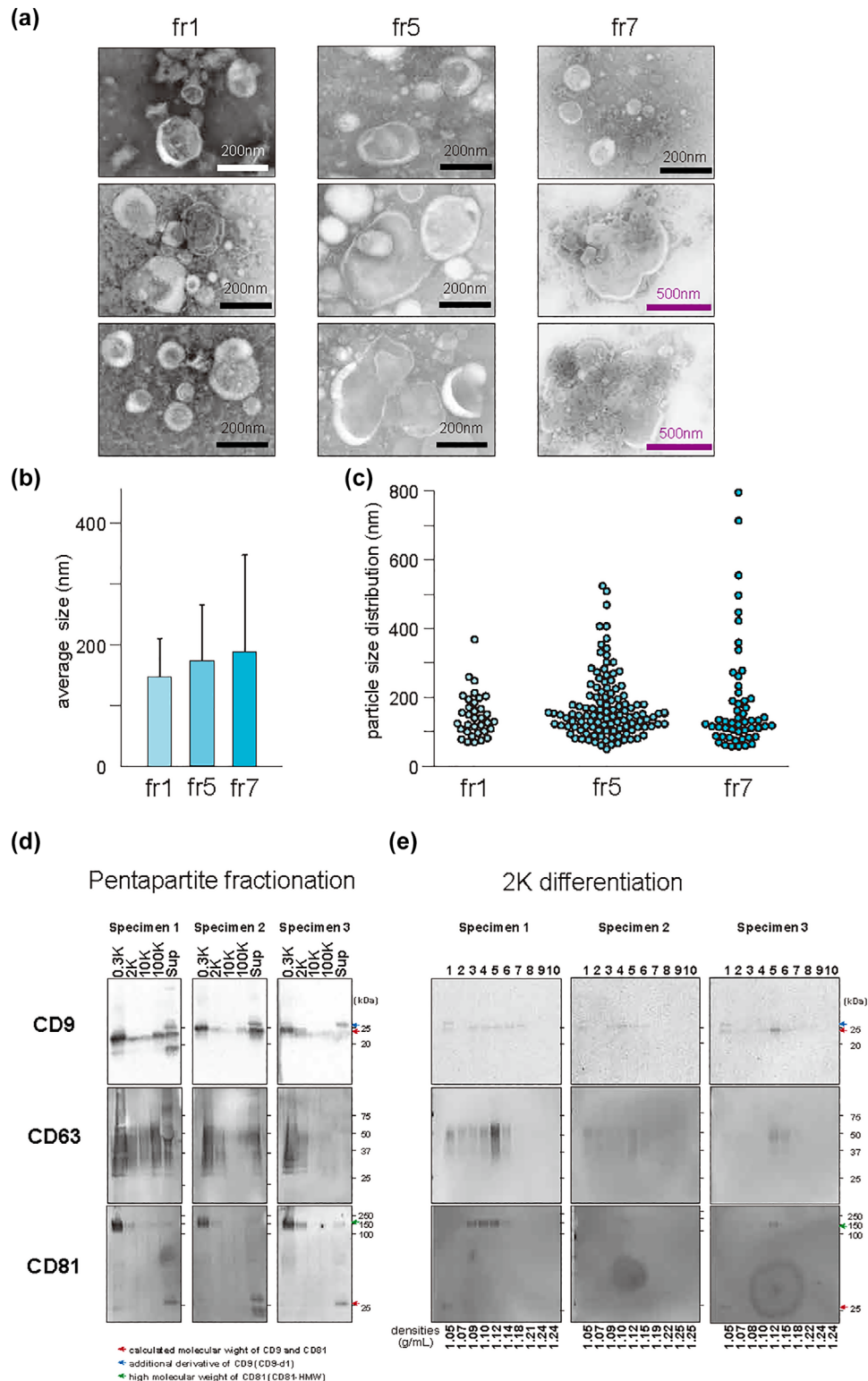


**FIGURE 2** TEM images of fractions 1, 5, and 7 and distribution of CD9, CD9-d, CD63, CD81, and CD81-HMW in pentapartite fractionation and non-equilibrium density gradient centrifugation followed by western blotting. (a) TEM images of fractions 1, 5, and 7 after centrifugation of the 2K fraction through an 8%–48% iodixanol density gradient at 2000 g for 1 h. The samples were stained with 2% phosphate tungstic acid. More than 20 images were taken for each fraction, and 3 representative images were shown. Note that the scale bar is 200 nm, but the scale of the middle and right columns of fraction 7 is 500 nm. (b) Mean particle size (nm) of each fraction calculated using ImageJ. Error bars indicate standard deviation. There was no statistically significant difference. (c) Graph showing the particle size distribution in fractions 1, 5 and 7. All fractions contained particles whose sizes were within the ranges of that of small EVs. (d) Western blots of CD9, CD63, and CD81 for the pentapartite fractions from OFs. (e) The 2K fractions were further differentiated by non-equilibrium density gradient centrifugation and proven with the same antibodies as (e). Numbers on the right of (d) and (e) show the molecular weights of markers. Red, blue, and green arrows indicate the calculated molecular weights of CD9 and CD81, an additional derivative of CD9 (CD9-d1), and the high molecular weight of CD81 (CD81-HMW), respectively. The origin of the CD81-HMW signal is discussed in Figure S5.



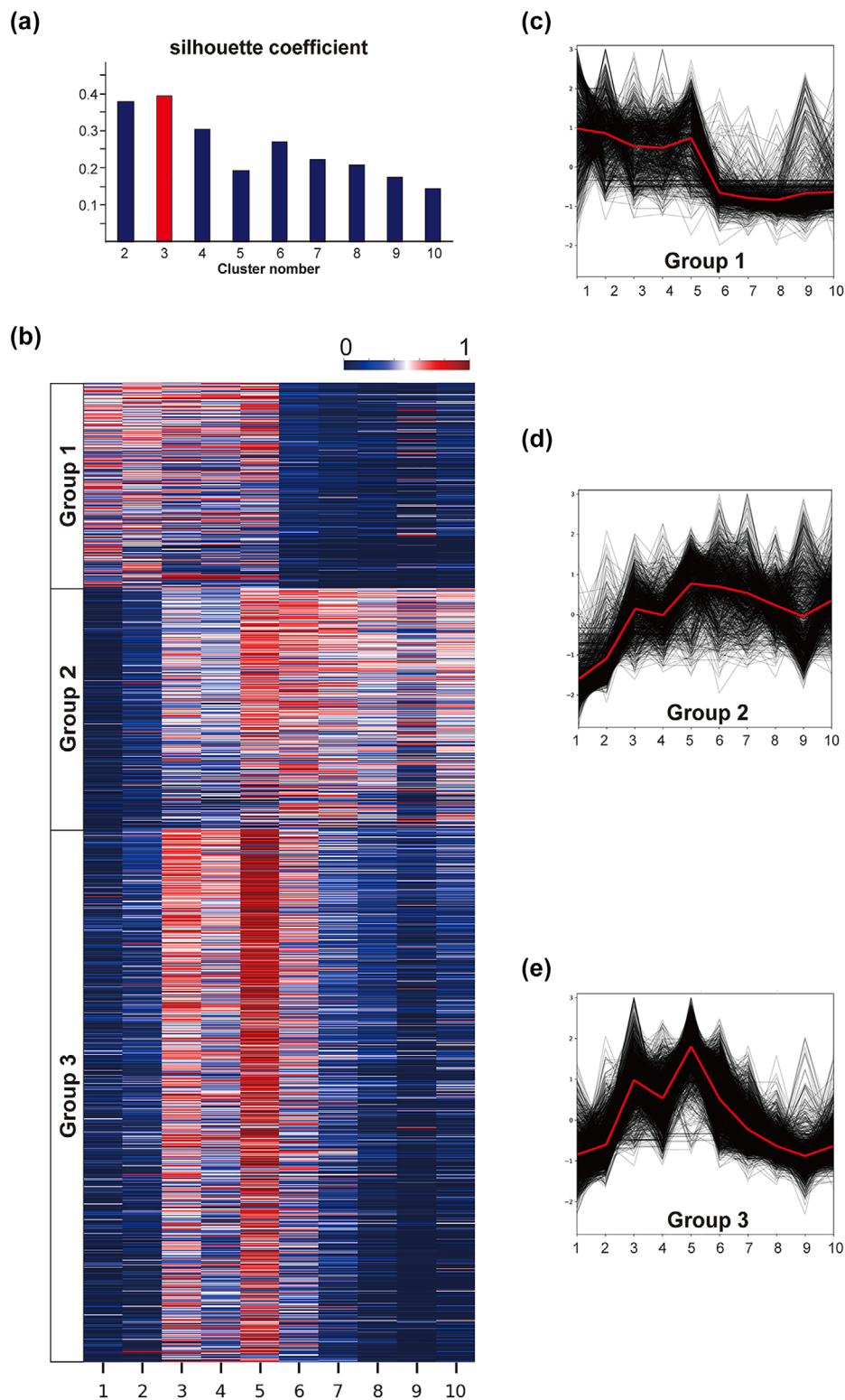


**FIGURE 3** Proteins in the 2K fraction cluster into three groups based on TimeSeriesKMeans algorithm. (a) Silhouette analysis estimated the best number of clusters. 3. The number at the axis of the ordinate represents silhouette coefficient of the Silhouette analysis. (b) Heatmap of proteins clustered into three by TimeSeriesKMeans. Each cluster is named Group 1, 2, and 3. Each coloured bar (total 3973) represents a single protein, and each row represents a fraction obtained from a non-equilibrium density gradient centrifugation. Expression per protein was normalized to 0 to 1. (c–e) Alternative representation of expression distribution among 10 fractions. Each black line represents individual proteins, which are shown for each group. The red lines represent the centroid of the group. (f) Subcellular localization of proteins included in each group, which were annotated with metascape, and only those with “enhanced” and “supported” levels of evidence were used. Yellow: endomembrane system; blue: cytoplasm; green: mitochondria; red: cell nuclei; gray: not identified. The number of proteins belonging to Groups 1, 2, and 3 are 833, 978 and 2162, respectively.

The three clusters calculated using TimeSeriesKMeans were “Group 1,” “Group 2,” and “Group 3,” each of which consisted of 833, 978 and 2162 proteins, respectively. Proteins belonging to Group 1 were mostly present in fractions 1–5; that is, they had a low sedimentation rate (Figure 3c, Table S1). The migration pattern of the proteins in Group 2 was complementary to that of Group 1 (Figure 3d, Table S1). The proteins classified as Group 3 had bipolar peaks in fractions 3 and 5 (Figure 3e, Table S1). We name this combination of a low speed, short time gradient centrifugation, and a non-hierarchical data clustering analysis *EV differentiation by sedimentation patterns* (ESP).

### 3.4 | ESP revealed three distinct functional groups of EVs in the 2K fraction

Proteins classified into three groups by ESP were annotated their subcellular localizations using metascape (Zhou et al., 2019), which confirmed the segregated properties of the three groups in terms of protein localizations. Group 2 was relatively enriched with the proteins located in the mitochondria, and group 1 contained fewer cytoplasmic and nuclear-localized proteins than others (Figure 4a). Next, using gene ontology analysis (Ashburner et al., 2000; Gene Ontology, 2021), the proteins of the three groups were classified from three perspectives: biological processes, cellular components, and molecular functions (Table S2). The top 20 Gene Ontology terms from these analyses were evaluated for their overlapping among the three groups (Figure 4b), which also indicated that the three groups were well segregated in terms of their cellular component, biological process, and molecular function (Figure 4b).

Next, we focused on a specific protein family, and we investigated the distribution of a group of proteins belonging to a certain protein family across the three groups (Figure 4c). Tetraspanins, including CD9, 63, and 81, which are often referred to as small EV markers but indeed are present in large EV fractions (Hiraga et al., 2021; Kowal et al., 2016), were enriched in Group 1 (**12/0/1**, representing the number of proteins belonging to Group 1/2/3, respectively). The most abundant group is shown in bold letters. The same applies hereinafter. Complete data are shown in Table S3). Integrins and a disintegrin and metalloproteinases (ADAMs) are proteins regarded as small EV markers in some reports, while others reported them to be present in both small and large EVs (Jeppesen et al., 2019; Kowal et al., 2016). These proteins also characterize Group 1 (**5/0/3** and **3/0/0**, respectively), other examples of which include those involved in immuno-related systems: immunoglobulins and HLA-Is were almost exclusively classified into Group 1 (**85/1/1**, and **3/0/0**, respectively). The 20S proteasome proteins, which are involved in processing antigenic peptides for the presentation by HLA-I (Goldberg & Rock, 1992), were also enriched in Group 1 (**11/5/0**). In Groups 2 and 3, the proteins involved in protein biosynthesis and energy metabolism were abundant, including cytoplasmic ribosomal proteins (**2/62/44**), mitochondrial ribosomal proteins (**0/48/29**), the heat shock 70 kDa protein family (**1/6/2**), electron transport system (**0/34/26**), citric acid cycle (**0/11/8**), and glycolytic system (**2/10/4**). The proteins involved in protein biosynthesis and energy metabolism are somewhat more prevalent in Group 2, but a considerable number of family proteins is also present in Group 3. Therefore, EVs containing these proteins may migrate during low-speed, short-time density gradient centrifugation with the patterns of Groups 2 and 3.

The fact that proteins engaging in protein biosynthesis and energy metabolism were biased toward both Groups 2 and 3 might suggest that Groups 1 and 2 are not well segregated by migration pattern-based analysis. However, when focusing on other protein families, it becomes evident that Groups 2 and 3 are indeed characterized by proteins with distinct functionalities: Protein families related to vesicle trafficking, such as Rabs (**5/9/22**), SNAREs (**3/2/9**), Kinesin-like proteins (**1/0/6**), and adaptor proteins (**3/1/15**), were all enriched in Group 3. The proteins categorized into the core autophagy system (Bordi et al., 2021) were also enriched in Group 3 (**4/20/61**). It should be noted that HSP90, which is known to stabilize Beclin-1 (Xu et al., 2011), a key regulator of autophagy, was enriched in Group-3 (**0/0/4**).

Overall, Groups 1, 2, and 3, which were classified based on their migration patterns following low-speed, short-time density gradient centrifugation, are characterized by the following properties: Group 1 was enriched with immuno-related proteins, and it shares EV marker proteins (tetraspanins and integrins) with small EVs, and Group 2 was characterized by protein biosynthesis and energy metabolism proteins. While Group 3 exhibits some of these proteins, its prominent characteristic was the enrichment of vesicle trafficking-related and autophagy-related proteins.

## 4 | DISCUSSION

The heterogeneity of EVs stem from (Théry et al., 2018) the differences in the parent cells from which they are derived, (Raposo et al., 1996) the differences in their generation pathways, and (Johnstone, 2005) the stochastic loading of cargos on the EVs. In the early phase of EV research in this decade, small EVs have gathered attention, often mentioned as generated through multivesicular bodies and uncritically named exosomes (Gould & Raposo, 2013). Thus, only the endosome-dependent pathway has been studied in relation to EV-generation pathways. However, recent studies have revealed that cells have a tremendous number of different systems that can produce EVs (Dixson et al., 2023; Théry et al., 2018). A comprehensive understanding of these pathways has not yet been achieved; however, some of the identified generation routes can be broadly categorized into three classes: (i) endosomal

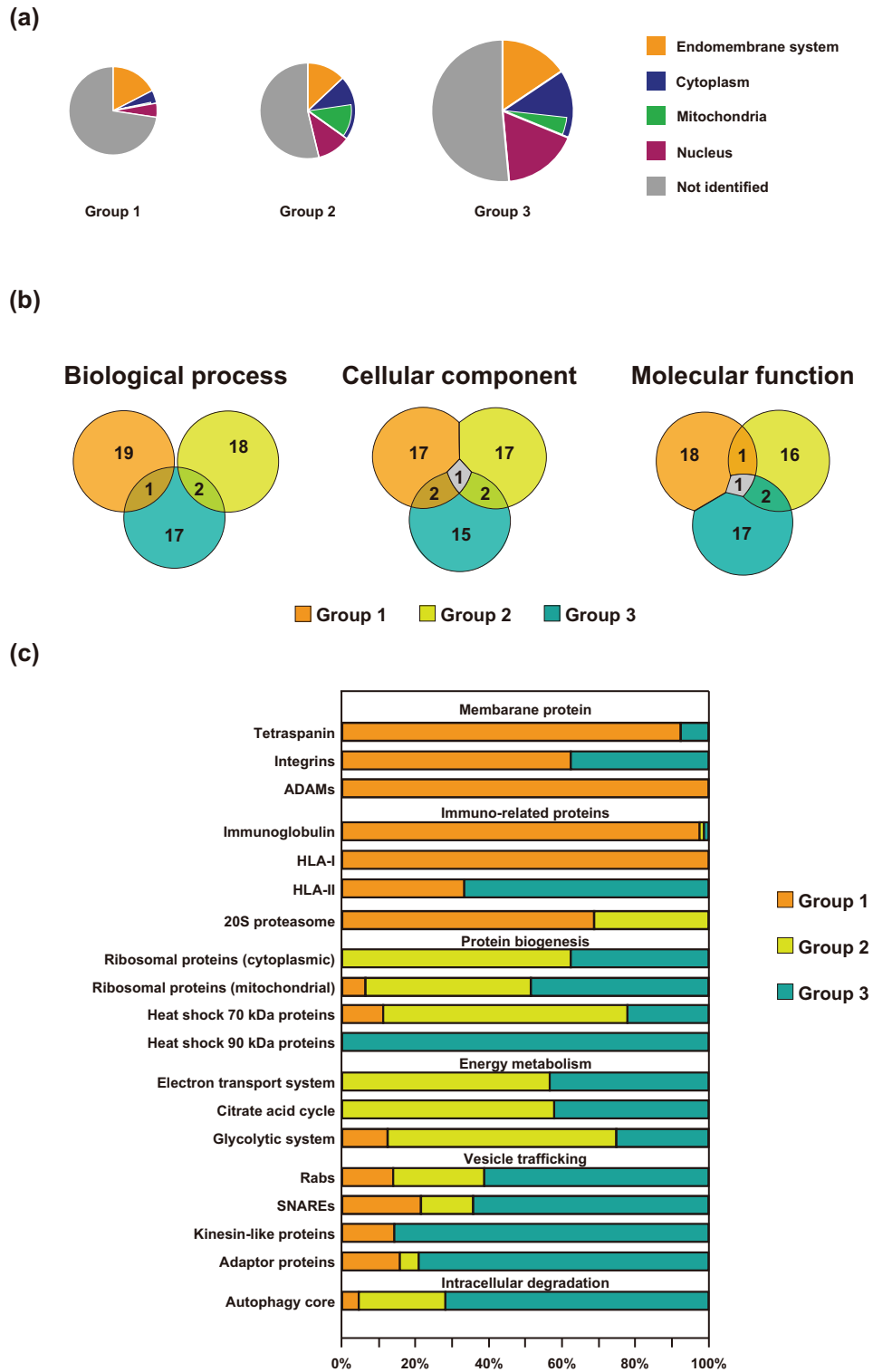


**FIGURE 4** Different biological functions are related to abundant proteins in Groups 1, 2, and 3. (a) Venn diagrams of results obtained from Gene Ontology enrichment analysis using top 20 proteins from each group (Supplementary Table 2). Metascape was used to annotate cellular components, biological processes, and molecular functions, and the overlaps between the groups are shown. (b) Distribution protein families among three groups are shown by bar graphs, which are grouped by protein family, that is, membrane protein, protein biogenesis, vesicle trafficking, intracellular degradation, immune, and energy metabolism. Orange: Group 1, yellow: Group 2, blue: Group 3.

organelle-dependent pathways (Johnstone, 2005; Raposo et al., 1996), (ii) protruded structure-derived pathways (Rilla, 2021; Sung et al., 2021), and (iii) regulated cell death pathways (Poon et al., 2019). These pathways produce EVs that have a wide range of sizes. For example, one of the regulated cell death pathways, apoptosis, is known to produce very large EVs, but the pathway also generates small EVs (Théry et al., 2001). Therefore, the size of EVs cannot sufficiently inform the routes responsible for their generation. Thus, the size fractionation of EVs is not solely sufficient for differentiating complex EV populations at high resolution. To solve this issue, equilibrium density gradient centrifugation has often been used to further differentiate crude small EV populations into their subclasses, depending on their densities (Raposo et al., 1996). In this methodology, size information of EVs is abandoned in the equilibrium state, which is not problematic in the case of small EVs because they have relatively uniform sizes. However, previous studies, including ours, have shown that the fraction that contains large EVs also include small EVs. Given that small EVs cannot be sedimented under typically centrifugation conditions (for instance, 2000 g for 10 min), they are somewhat associated with larger entities (or artificially generated during the EV preparation process). The coexistence of small EVs and large EVs in large EV fractions encouraged us to separate these EVs under the non-equilibrium conditions of density gradient centrifugation so that the size information would contribute to the differentiation.

When the 2K fraction of OFs was sedimented through a gradient of iodixanol under the conditions of 2000 g for 1 h, small EVs remained in the top fractions, and large EVs migrated to the middle position, enabling separation of the size different EVs. Interestingly, TEM observations indicated that the fractions of large EVs (fast migrating fractions) also contained large numbers of small EVs. This fact supports the possibility that small EVs became bound to large EVs and behaved as larger particles during centrifugation. Some portions were detached from the complex and acted as free small particles. However, as shown in this study, the origins of the small EV in the large EV fraction were much more complex. For instance, western blotting results showed that CD9 and CD81 are present in different forms in terms of their apparent molecular weight (Figure 2d). CD9 gave the additional signal that had a slightly higher molecular weight; CD9-d1 and anti-CD81 antibody detected the high molecular weight CD81-HMW. Previous studies have reported that CD9 has its palmitoylated form (Charrin et al., 2002; Umeda et al., 2019), which may correspond to CD9-d1. The CD81-HMW was only detected in OF but not from plasma samples or the conditioned medium of cell lines (unpublished data) and was detected in some OF specimens. Both CD81 and CD81-HMW were recognized by two different antibodies, SHI-EXO-M03 and 66866-1-Ig (whose epitopes are residues 35–54 and 114–199 of CD81, respectively) (Figure S5A), excluding the possibility that the signal was antibody-specific background noise. Given that CD81 has been known to act as a chaperone for CD19 (Shoham et al., 2003), we evaluated the possibility that CD81-HMW contains CD9 as a component; however, western blotting with anti-CD19 has shown that this is not the case (Figure S5B). Glycosylation is one possibility that could have increased the molecular weight of CD81, although no study has reported the existence of glycosylated forms of CD81. Treatments of the 2K fraction with PNGaseF or O-glycosidase, which cleaves N-linked glycans or O-linked glycans from glycoproteins, respectively, did not decrease the apparent molecular weight of CD81-HMW (Figure S5C–E), dismissing the possibility that heavy glycosylation of CD81 increased the molecular weight. Quite a few membranous proteins have been reported to migrate anomalously in SDS-PAGE. In some cases, heat treatment of a sample that is included in a standard SDS-PAGE protocol has an adverse effect on the results (Ito, 1984). To investigate the effect of heat treatment, the proteins in 2K were separated by diagonal 2D SDS-PAGE, which was used to detect the effects of thermal denaturation (Figure S5F–K) (Xia et al., 2017). Diagonal migration of proteins indicated that the CD81-HMW was not an artifact generated during sample preparation (for more detailed discussion, see legend of Figure S5). Although the origin of CD81-HMW is not explained by previously known mechanisms, two molecular forms of CD81 and CD9 provide valuable clues as to the nature of the small EVs in the large EV fraction. As shown in the Figure 2(e), when the 2K fraction was developed by a non-equilibrium density gradient, two forms of these proteins were segregated into different fractions: CD9-d1 and CD81 remained in fraction 1, and CD9 and CD81-HMW moved to fractions containing large EVs. Since the large EV fraction contained many small EVs (Figure 2c), the segregation of two forms of CD9 and CD81 ruled out the simple scenario in which small EVs become bound to the surfaces of large EVs and some small EVs behaved as larger particles and others acted as free particles after detaching from large EV in the centrifugation. With the current observations, we could not rule out the improbable possibility that CD9 and CD81-HMW in fractions 3 to 5 stemmed only from large EVs but not from small EVs. Considering the fact that the small EVs in the small EV crude fraction (I60K) have been further differentiated into several subclasses, distinct types of small EVs exist in OFs not only in the small EV fraction but also in the large EV fraction.

Non-equilibrium density gradient centrifugation at 2000 g for 1 h separates EVs based on their sizes and densities. As discussed above, a single EV-generation pathway could produce various sizes of EVs, and most probably, with various densities. However, we were interested in the possibility that certain EV-generation pathways might have characteristic distributions of sizes or densities of EVs (for instance, one pathway always produces both small and large EVs, the other generates a large and high density of EVs, and so on). Therefore, we intended to elucidate the characteristic patterns of molecular distributions in non-equilibrium density gradient centrifugation. We named this combination of biochemical separation and data analysis *EV differentiation by sedimentation patterns* (ESP). After separation of entities in the 2K fraction into 10 fractions with a low speed and short time gradient centrifugation, the proteins contained in each fraction were identified by MS. Standard clustering analyses of MS data did not detect prominent groupings of the segregated proteins (Figure S4). However, when the data were analysed by TimeSeriesKMeans, three well-separated groups were revealed (Figure 3b). TimeSeriesKMeans is an algorithm that has been developed for clustering

high-dimensional data and possesses high performance in searching patterns from data (Tavenard et al., 2020). The proteins that were sorted into Group 1 were abundant in fractions 1 to 5, which included many membrane proteins, such as CD9, CD63, CD81, and ADAMs. Proteins involved in protein biosynthesis and energy metabolism were enriched in Group 2, and they were moved to fractions 5–10. In Group 3, the proteins involved in protein biosynthesis and energy metabolism were also present, but they are distinguished from Group 2 via protein enrichment related to vesicle trafficking and autophagy. The migration pattern of Group 3 demonstrated bipolar peaks in fractions 3 and 5 (Figure 3c–e).

Yamamoto et al. performed proteomic analysis of OFs' fractions that contained medium and small EVs (Yamamoto et al., 2021). Comparison of proteome results from these two data provides information about overlapping and independency between the crude large EV fraction and the crude medium and small EV fraction (Figure S7). Among these fractions, 961 out of 3973 (this study) and 1429 (Yamamoto et al. (Yamamoto et al., 2021)) proteins overlapped, among which 421, 210, and 330 proteins belonged to Groups 1, 2, and 3 were identified in this study (Figure S6). In other words, half of the proteins that were sorted into Group 1 were also present in middle to small EVs, while the majority of proteins classified into Groups 2 and 3 were specific to the 2K fraction. In previous studies, proteomic analysis and western blotting showed that mitofilin was enriched in large EVs compared to small EVs (Crescitelli et al., 2020; Kowal et al., 2016), and ADAM10 was enriched in low-density small EVs (Crescitelli et al., 2020). In this study, mitofilin was distributed in Group 2, which contains many proteins specific to the 2K fraction, and ADAM10 belonged to Group 1, which contains many proteins that have also been used as small EV markers (Kowal et al., 2016). Mitofilin was not detected in the experiment by Yamamoto et al. (Yamamoto et al., 2021). ACTN4 (Kowal et al., 2016), and ANXA1 (Jeppesen et al., 2019) were reported as large EV markers, and they were classified into Group 2. From these data, Group 2 and Group 3 proteins have characteristic features of the large EV fraction. When these proteins were assigned their annotated characters, we found functional relationships between Group 1 and immuno-related and membrane proteins, Group 2 and energy metabolism and translation, and Group 3 and vesicle trafficking. These correlations potentially illustrate the distinct biogenesis pathways of EVs, enriching our strategies for potential clinical interventions. For example, when leveraging EVs for immune modulation, a focus on protein molecules classified under Group 1 is pivotal in designing experimental systems, thereby advancing the development of precise and effective EV-based treatments. It is also reasonable to believe that data obtained from similar analyses using singular cell types, such as cultured cells, will deepen our understanding of the relationships between the large subtypes of EVs found in complex body fluids, their cell types of origin, and their biogenesis pathways.

In the pentapartite fractionation by Hiraga et al. (Hiraga et al., 2021), the Sup fraction, the final supernatant, was for western blotting without concentration, making it difficult to directly compare the abundance of proteins between the EV fractions and supernatant. In this study, we modified the pentapartite fractionation protocol to concentrate Sup so that a more intuitive visual comparison was possible. Interestingly, the concentrated Sup demonstrated a comparable or even stronger signal than the 100K fraction for CD9, CD63, and CD81 (Figure 2d). Recent studies have revealed that exomeres (Zhang et al., 2018) and supermeres (Zhang et al., 2021) also carry these molecules, which are tiny particles recovered in supernatant fractions in standard EV preparation protocol and, based on MISEV definition of EV, are non-EV particles because they do not have typical lipid bilayers found in vesicles. Thus, CD9, CD63, and CD81, which used to be regarded as small EV markers, are widely distributed among various particles in bodily fluids. However, as shown in this work and in previous work, some of their derivatives (such as CD9-dl or CD81-HMW) show varied distributions, which may contribute to the development of EV-based diagnosis (Al-Nedawi et al., 2008).

In previous studies, heterogeneous EVs have been subtyped by their apparent size through differential centrifugation and/or by intrinsic density through equilibrium density gradient. However, accumulated knowledge suggests that EVs generated through a particular pathway do not necessarily exhibit characteristic sizes or densities. Hence, to elucidate a comprehensive understanding of EV subtypes, devising differential methods from new perspectives is crucial. Within this context, ESP focuses on the “segregation pattern” of EVs within the centrifugation media and classifies EVs into three groups based on this pattern. As a result, proteins belonging to each of the classified groups appear to correspond to distinctive biological functions, revealing a possibility that the physicochemical properties of EVs (that must be reflected in their migration pattern) are associated with their functions within cells, suggesting the potential utilization of ESP as a method for subtyping EVs and offering an alternative to previous approaches.

## AUTHOR CONTRIBUTIONS

**Takamasa Kawano:** Conceptualization; data curation; formal analysis; investigation; methodology; software; validation; visualization; writing—original draft. **Kohji Okamura:** Software. **Hiroki Shinchi:** Investigation; methodology. **Koji Ueda:** Investigation; methodology. **Takeshi Nomura:** Project administration; supervision. **Kiyotaka Shiba:** Conceptualization; data curation; funding acquisition; investigation; methodology; project administration; supervision; writing—original draft; writing—review and editing.

## ACKNOWLEDGEMENTS

This work was supported by JSPS Grant-in-Aid for Scientific Research (B) with KAKENHI Grant Number 20H03538. The authors thank C. Hiraga (Tokyo Dental College) and T. Minamisawa (Japanese Foundation for Cancer Research) for their helpful discussions. The authors acknowledge NOF Corporation for providing Lipidure-BL802.

## CONFLICT OF INTEREST STATEMENT

The authors declare no conflicts of interest.

## ORCID

Kiyotaka Shiba  <https://orcid.org/0000-0001-6459-0204>

## REFERENCES

- Aalberts, M., van Dissel-Emiliani, F. M., van Adrichem, N. P., van Wijnen, M., Wauben, M. H., Stout, T. A., & Stoorvogel, W. (2012). Identification of distinct populations of prostasomes that differentially express prostate stem cell antigen, annexin A1, and GLIPR2 in humans. *Biology of Reproduction*, *86*, 82.
- Al-Nedawi, K., Meehan, B., Micallef, J., Lhotak, V., May, L., Guha, A., & Rak, J. (2008). Intercellular transfer of the oncogenic receptor EGFRvIII by microvesicles derived from tumour cells. *Nature Cell Biology*, *10*, 619–624.
- Anderson, H. C. (1969). Vesicles associated with calcification in the matrix of epiphyseal cartilage. *Journal of Cell Biology*, *41*, 59–72.
- Ashburner, M., Ball, C. A., Blake, J. A., Botstein, D., Butler, H., Cherry, J. M., Davis, A. P., Dolinski, K., Dwight, S. S., Eppig, J. T., & Harris, M. A. (2000). Gene ontology: Tool for the unification of biology. The Gene Ontology Consortium. *Nature Genetics*, *25*, 25–29.
- Bedre, R. (2020). Reneshbedre/Bioinfokit: Bioinformatics data analysis and visualization toolkit. *Zenodo*, <https://doi.org/10.5281/zenodo.3841708>
- Bordi, M., De Cegli, R., Testa, B., Nixon, R. A., Ballabio, A., & Cecconi, F. (2021). A gene toolbox for monitoring autophagy transcription. *Cell Death and Disease*, *12*, 1044.
- Brody, I., Ronquist, G., & Gottfries, A. (1983). Ultrastructural localization of the prostasome—An organelle in human seminal plasma. *Upsala Journal of Medical Sciences*, *88*, 63–80.
- Buzas, E. I. (2023). The roles of extracellular vesicles in the immune system. *Nature Reviews Immunology*, *23*, 236–250.
- Carr, B., Hole, P., Malloy, A., Nelson, P., & Smith, J. (2009). Applications of nanoparticle tracking analysis in nanoparticle research—A mini-review. *European Journal of Parenteral and Pharmaceutical Sciences*, *14*, 45.
- Charrin, S., Manié, S., Oualid, M., Billard, M., Boucheix, C., & Rubinstein, E. (2002). Differential stability of tetraspanin/tetraspanin interactions: Role of palmitoylation. *FEBS Letters*, *516*, 139–144.
- Colombo, M., Raposo, G., & Théry, C. (2014). Biogenesis, secretion, and intercellular interactions of exosomes and other extracellular vesicles. *Annual Review of Cell and Developmental Biology*, *30*, 255–289.
- Crescitelli, R., Lässer, C., Jang, S. C., Cvjetkovic, A., Malmhäll, C., Karimi, N., Höög, J. L., Johansson, I., Fuchs, J., Thorsell, A., & Ghossein, Y. S. (2020). Subpopulations of extracellular vesicles from human metastatic melanoma tissue identified by quantitative proteomics after optimized isolation. *Journal of Extracellular Vesicles*, *9*, 1722433.
- Dixon, A. C., Dawson, T. R., Di Vizio, D., & Weaver, A. M. (2023). Context-specific regulation of extracellular vesicle biogenesis and cargo selection. *Nature Reviews Molecular Cell Biology*, *24*, 454–476. <https://doi.org/10.1038/s41580-023-00576-0>
- Dragovic, R. A., Gardiner, C., Brooks, A. S., Tannetta, D. S., Ferguson, D. J., Hole, P., Carr, B., Redman, C. W., Harris, A. L., Dobson, P. J., & Harrison, P. (2011). Sizing and phenotyping of cellular vesicles using nanoparticle tracking analysis. *Nanomedicine*, *7*, 780–788.
- Gene Ontology, C. (2021). The Gene Ontology resource: Enriching a GOld mine. *Nucleic Acids Research*, *49*, D325–D334.
- Goldberg, A. L., & Rock, K. L. (1992). Proteolysis, proteasomes and antigen presentation. *Nature*, *357*, 375–379.
- Gould, S. J., & Raposo, G. (2013). As we wait: Coping with an imperfect nomenclature for extracellular vesicles. *Journal of Extracellular Vesicles*, *2*, 20389.
- Harris, C. R., Millman, K. J., Van Der Walt, S. J., Gommers, R., Virtanen, P., Cournapeau, D., Wieser, E., Taylor, J., Berg, S., Smith, N. J., & Kern, R. (2020). Array programming with NumPy. *Nature*, *585*, 357–362.
- Hiraga, C., Yamamoto, S., Hashimoto, S., Kasahara, M., Minamisawa, T., Matsumura, S., Katakura, A., Yajima, Y., Nomura, T., & Shiba, K. (2021). Pentapartite fractionation of particles in oral fluids by differential centrifugation. *Science Reports*, *11*, 3326.
- Hunter, J. D. (2007). Matplotlib: A 2D graphics environment. *Computing in Science and Engineering*, *9*, 90–95.
- Ishikawa, Y., & Ishida, H. (2000). Aquaporin water channel in salivary glands. *Japanese Journal of Pharmacology*, *83*, 95–101.
- Ito, K. (1984). Identification of the *secY* (*prlA*) gene product involved in protein export in *Escherichia coli*. *Molecular Genetics and Genomics*, *197*, 204–208.
- Iwai, K., Minamisawa, T., Suga, K., Yajima, Y., & Shiba, K. (2016). Isolation of human salivary extracellular vesicles by iodixanol density gradient ultracentrifugation and their characterizations. *Journal of Extracellular Vesicles*, *5*, 30829.
- Jeppesen, D. K., Fenix, A. M., Franklin, J. L., Higginbotham, J. N., Zhang, Q., Zimmerman, L. J., Liebler, D. C., Ping, J., Liu, Q., Evans, R., & Fissell, W. H. (2019). Reassessment of exosome composition. *Cell*, *177*, 428–445.
- Johnstone, R. M. (2005). Revisiting the road to the discovery of exosomes. *Blood Cells, Molecules and Diseases*, *34*, 214–219.
- Kilinc, S., Paisner, R., Camarda, R., Gupta, S., Momcilovic, O., Kohnz, R. A., Avsaroglu, B., Noelle, D. L., Perera, R. M., Nomura, D. K., & Goga, A. (2021). Oncogene-regulated release of extracellular vesicles. *Developmental Cell*, *56*, 1989–2006. e1986.
- Kowal, J., Arras, G., Colombo, M., Jouve, M., Morath, J. P., Primald-Bengtson, B., Dingli, F., Loew, D., Tkach, M., & Théry, C. (2016). Proteomic comparison defines novel markers to characterize heterogeneous populations of extracellular vesicle subtypes. *Proceedings of National Academy of Sciences USA*, *113*, E968–E977.
- Linares, R., Tan, S., Gounou, C., Arraud, N., & Brisson, A. R. (2015). High-speed centrifugation induces aggregation of extracellular vesicles. *Journal of Extracellular Vesicles*, *4*, 29509.
- Lischinig, A., Bergqvist, M., Ochiya, T., & Lasser, C. (2022). Quantitative proteomics identifies proteins enriched in large and small extracellular vesicles. *Molecular and Cellular Proteomics*, *21*, 100273.
- Melentijevic, I., Toth, M. L., Arnold, M. L., Guasp, R. J., Harinath, G., Nguyen, K. C., Taub, D., Parker, J. A., Neri, C., Gabel, C. V., & Hall, D. H. (2017). *C. elegans* neurons jettison protein aggregates and mitochondria under neurotoxic stress. *Nature*, *542*, 367–371.
- Nonaka, T., & Wong, D. T. W. (2017). Saliva-exosomics in cancer: Molecular characterization of cancer-derived exosomes in saliva. *Enzymes*, *42*, 125–151.

- Palma, J., Yaddanapudi, S. C., Pigati, L., Havens, M. A., Jeong, S., Weiner, G. A., Weimer, K. M. E., Stern, B., Hastings, M. L., & Duelli, D. M. (2012). MicroRNAs are exported from malignant cells in customized particles. *Nucleic Acids Research*, *40*, 9125–9138.
- Pedregosa, F. (2011). Scikit-learn: Machine learning in Python. *Journal of Machine Learning Research*, *2*, 2825–2830.
- Poon, I. K., Parkes, M. A., Jiang, L., Atkin-Smith, G. K., Tixeira, R., Gregory, C. D., Ozkocak, D. C., Rutter, S. F., Caruso, S., Santavanond, J. P., & Paone, S. (2019). Moving beyond size and phosphatidylserine exposure: Evidence for a diversity of apoptotic cell-derived extracellular vesicles *in vitro*. *Journal of Extracellular Vesicles*, *8*, 1608786.
- Raposo, G., Nijman, H. W., Stoorvogel, W., Liejendekker, R., Harding, C. V., Melief, C. J., & Geuze, H. J. (1996). B lymphocytes secrete antigen-presenting vesicles. *Journal of Experimental Medicine*, *183*, 1161–1172.
- Reback, J., McKinney, W., Van Den Bossche, J., Augspurger, T., Cloud, P., Klein, A., Hawkins, S., Roeschke, M., Tratner, J., She, C., & Ayd, W. (2020). pandas-dev/pandas: Pandas 1.0. 5. Zenodo.
- Rilla, K. (2021). Diverse plasma membrane protrusions act as platforms for extracellular vesicle shedding. *Journal of Extracellular Vesicles*, *10*, e12148.
- Ropolo, A., Grasso, D., Pardo, R., Sacchetti, M. L., Archange, C., Re, A. L., Seux, M., Nowak, J., Gonzalez, C. D., Iovanna, J. L., & Vaccaro, M. I. (2007). The pancreatitis-induced vacuole membrane protein 1 triggers autophagy in mammalian cells. *Journal of Biological Chemistry*, *282*, 37124–37133.
- Rousseeuw, P. J. (1987). Silhouettes: A graphical aid to the interpretation and validation of cluster analysis. *Journal of Computational and Applied Mathematics*, *20*, 53–65.
- Salomon, C., Das, S., Erdbrügger, U., Kalluri, R., Kiang Lim, S., Olefsky, J. M., Rice, G. E., Sahoo, S., Andy Tao, W., Vader, P., & Wang, Q. (2022). Extracellular vesicles and their emerging roles as cellular messengers in endocrinology: An Endocrine Society Scientific Statement. *Endocrine Reviews*, *43*, 441–468.
- Shoham, T., Rajapaksa, R., Boucheix, C., Rubinstein, E., Poe, J. C., Tedder, T. F., & Levy, S. (2003). The tetraspanin CD81 regulates the expression of CD19 during B cell development in a postendoplasmic reticulum compartment. *Journal of Immunology*, *171*, 4062–4072.
- Sung, B. H., Parent, C. A., & Weaver, A. M. (2021). Extracellular vesicles: Critical players during cell migration. *Developmental Cell*, *56*, 1861–1874.
- Tavenard, R., Faouzi, J., Vandewiele, G., Divo, F., Androz, G., Holtz, C., Payne, M., Yurchak, R., Rufswurm, M., Kolar, K., & Woods, E. (2020). Tslearn, a machine learning toolkit for time series data. *Journal of Machine Learning Research*, *21*, 1–6.
- Théry, C., Boussac, M., Véron, P., Ricciardi-Castagnoli, P., Raposo, G., Garin, J., & Amigorena, S. (2001). Proteomic analysis of dendritic cell-derived exosomes: A secreted subcellular compartment distinct from apoptotic vesicles. *Journal of Immunology*, *166*, 7309–7318.
- Théry, C., Witwer, K. W., Aikawa, E., Alcaraz, M. J., Anderson, J. D., Andriantsitohaina, R., Antoniou, A., Arab, T., Archer, F., Atkin-Smith, G. K., & Ayre, D. C. (2018). Minimal information for studies of extracellular vesicles 2018 (MISEV2018): A position statement of the International Society for Extracellular Vesicles and update of the MISEV2014 guidelines. *Journal of Extracellular Vesicles*, *7*, 1535750.
- Umeda, R., Nishizawa, T., & Nureki, O. (2019). Crystallization of the human tetraspanin protein CD9. *Acta Crystallographica F Structural Biology Communications*, *75*, 254–259.
- Valcz, G., Buzás, E. I., Kittel, Á., Krenács, T., Visnovitz, T., Spisák, S., Török, G., Homolya, L., Zsigrai, S., Kiszler, G., & Antalffy, G. (2019). *En bloc* release of MVB-like small extracellular vesicle clusters by colorectal carcinoma cells. *Journal of Extracellular Vesicles*, *8*, 1596668.
- Van der Pol, E., Coumans, F. A. W., Grootemaat, A. E., Gardiner, C., Sargent, I. L., Harrison, P., Sturk, A., Van Leeuwen, T. G., & Nieuwland, R. (2014). Particle size distribution of exosomes and microvesicles determined by transmission electron microscopy, flow cytometry, nanoparticle tracking analysis, and resistive pulse sensing. *Journal of Thrombosis and Haemostasis*, *2*, 1182–1192.
- Van Deun, J., Mestdagh, P., Agostinis, P., Akay, Ö., Anand, S., Anckaert, J., Martinez, Z. A., Baetens, T., Beghein, E., Bertier, L., & Berx, G. (2017). EV-TRACK: Transparent reporting and centralizing knowledge in extracellular vesicle research. *Nature Methods*, *14*, 228–232.
- van Niel, G., D'Angelo, G., & Raposo, G. (2018). Shedding light on the cell biology of extracellular vesicles. *Nature Reviews Molecular Cell Biology*, *9*, 213–228.
- Virtanen, P., Gommers, R., Oliphant, T. E., Haberland, M., Reddy, T., Cournapeau, D., Burovski, E., Peterson, P., Weckesser, W., Bright, J., & Van Der Walt, S. J. (2020). SciPy 1.0: Fundamental algorithms for scientific computing in Python. *Nature Methods*, *17*, 261–272.
- Waskom, M. L. (2021). Seaborn: Statistical data visualization. *Journal of Open Source Software*, *6*, 3021.
- Weems, A. D., Welf, E. S., Driscoll, M. K., Zhou, F. Y., Mazloom-Farsibaf, H., Chang, B. J., Murali, V. S., Gihana, G. M., Weiss, B. G., Chi, J., & Rajendran, D. (2023). Blebs promote cell survival by assembling oncogenic signalling hubs. *Nature*, *615*, 517–525.
- Xia, K., Manning, M., Hesham, H., Lin, Q., Byströf, C., & Colón, W. (2017). Identifying the subproteome of kinetically stable proteins via diagonal 2D SDS/PAGE. *Proceedings of National Academy of Science USA*, *104*, 17329–17334.
- Xu, C., Liu, J., Hsu, L. C., Luo, Y., Xiang, R., & Chuang, T. H. (2011). Functional interaction of heat shock protein 90 and Beclin 1 modulates Toll-like receptor-mediated autophagy. *FASEB Journal*, *25*, 2700–2710.
- Xu, R., Greening, D. W., Zhu, H. J., Takahashi, N., & Simpson, R. J. (2016). Extracellular vesicle isolation and characterization: Toward clinical application. *Journal of Clinical Investigation*, *126*, 1152–1162.
- Yamamoto, S., Okamura, K., Fujii, R., Kawano, T., Ueda, K., Yajima, Y., & Shiba, K. (2021). Specimen-specific drift of densities defines distinct subclasses of extracellular vesicles from human whole saliva. *PLoS ONE*, *16*, e0249526.
- Zhang, H., Freitas, D., Kim, H. S., Fabijanic, K., Li, Z., Chen, H., Mark, M. T., Molina, H., Martin, A. B., Bojmar, L., & Fang, J. (2018). Identification of distinct nanoparticles and subsets of extracellular vesicles by asymmetric flow field-flow fractionation. *Nature Cell Biology*, *20*, 332–343.
- Zhang, Q., Jeppesen, D. K., Higginbotham, J. N., Graves-Deal, R., Trinh, V. Q., Ramirez, M. A., Sohn, Y., Neiningner, A. C., Taneja, N., McKinley, E. T., & Niitsu, H. (2021). Supermeres are functional extracellular nanoparticles replete with disease biomarkers and therapeutic targets. *Nature Cell Biology*, *23*, 1240–1254.
- Zhou, Y., Zhou, B., Pache, L., Chang, M., Khodabakhshi, A. H., Tanaseichuk, O., Benner, C., & Chanda, S. K. (2019). Metascape provides a biologist-oriented resource for the analysis of systems-level datasets. *Nature Communications*, *10*, 1523.

## SUPPORTING INFORMATION

Additional supporting information can be found online in the Supporting Information section at the end of this article.

**How to cite this article:** Kawano, T., Okamura, K., Shinchi, H., Ueda, K., Nomura, T., & Shiba, K. (2024). Differentiation of Large Extracellular Vesicles in Oral Fluid: Combined Protocol of Small Force Centrifugation and Sedimentation Pattern Analysis. *Journal of Extracellular Biology*, *3*, e143. <https://doi.org/10.1002/jex2.143>